Photoacoustics 25 (2022) 100326

Contents lists available at ScienceDirect

Photoacoustics

journal homepage: www.elsevier.com/locate/pacs

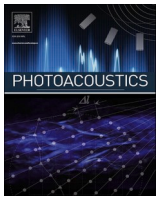

Photoacoustic imaging of squirrel monkey cortical and subcortical brain regions during peripheral electrical stimulation

Kai-Wei Chang [a,1], Yunhao Zhu [a,1], Heather M. Hudson [b], Scott Barbay [b,c], David J. Guggenmos [b,c], Randolph J. Nudo [b,c,*], Xinmai Yang [d,**], Xueding Wang [a,**]

[a] Department of Biomedical Engineering, University of Michigan, Ann Arbor, MI 48109, United States
[b] Landon Center on Aging, University of Kansas Medical Center, Kansas City, KS 66160, United States
[c] Department of Rehabilitation Medicine, University of Kansas Medical Center, Kansas City, KS 66160, United States
[d] Department of Mechanical Engineering and Institute for Bioengineering Research, University of Kansas, Lawrence, KS 66045, United States

ARTICLE INFO

Keywords:
Non-human primate
Photoacoustic imaging
Photoacoustic computed tomography
Photoacoustic microscopy
Peripheral electrical stimulation

ABSTRACT

The investigation of neuronal activity in non-human primate models is of critical importance due to their genetic similarity to human brains. In this study, we tested the feasibility of using photoacoustic imaging for the detection of cortical and subcortical responses due to peripheral electrical stimulation in a squirrel monkey model. Photoacoustic computed tomography and photoacoustic microscopy were applied on squirrel monkeys for real-time deep subcortical imaging and optical-resolution cortical imaging, respectively. The electrically evoked hemodynamic changes in primary somatosensory cortex, premotor cortices, primary motor cortex, and underlying subcortical areas were measured. Hemodynamic responses were observed in both cortical and subcortical brain areas at the cortices during external stimulation, demonstrating the feasibility of photoacoustic technique for functional imaging of non-human primate brain.

1. Introduction

Non-human primates (NHPs) play a significant role in medical and scientific advances, especially in brain research. Because of the physiological similarities between humans and NHPs, animal models based on NHPs can address questions that cannot be addressed using other species [1]. Development of functional imaging methods that can be applied to the NHP brain is vital for understanding of brain functions and has the potential for relevance to a wide range of neurological conditions such as stroke, Alzheimer's disease, Parkinson's disease and epilepsy [2,3].

Studies using invasive neurophysiological electrical recording techniques in NHPs have provided knowledge about the functional organization of the primate brain. However, electrical recording using microelectrodes is quite invasive. Though it can provide good spatial resolution and depth-resolved information, it is confined to only a limited expanse of tissue at one time. Hence, electrical recording techniques can only offer limited information in primate-based brain mapping, and are very difficult to utilize when deep brain functional information is desired. Subcortical structures located a few centimeters below the cortex play a pivotal role not only in sensorimotor processing, but also in cognitive, affective and social functions associated with various psychiatric disorders including schizophrenia, depression, and autism spectrum disorders [4]. Currently, it is largely unknown how abnormalities of specific subcortical nuclei are associated with neurocognitive and socio-functional consequences.

Functional magnetic resonance imaging (fMRI) has been widely used to detect functional changes simultaneously throughout the entire brain [5–10]. However, this technique is associated with high cost and limited temporal and spatial resolution when collecting functional information. Particularly, for brain research involving awake, behaviorally active monkeys, the limited temporal resolution of fMRI can be a significant barrier for obtaining accurate functional information because of motion artifacts [11–13]. Although human MRI scanner has been applied in NHP research, significant technical challenges such as motion artifacts remain to be solved [14,15]. Even with anesthesia, it is not possible to

* Corresponding author at: Landon Center on Aging, University of Kansas Medical Center, Kansas City, KS 66160, United States.
** Corresponding authors.
E-mail addresses: rnudo@kumc.edu (R.J. Nudo), xmyang@ku.edu (X. Yang), xdwang@umich.edu (X. Wang).
[1] These authors contributed equally to this work.

https://doi.org/10.1016/j.pacs.2021.100326
Received 9 August 2021; Received in revised form 18 November 2021; Accepted 16 December 2021
Available online 17 December 2021

completely eliminate the motion artifacts in fMRI due to cardiac and respiration cycles.

Optical brain imaging can provide complementary information to other modalities such as microelectrode recordings and fMRI, and provides a low-cost alternative in many settings [16–23]. Furthermore, optical imaging can be performed in real time, opening up new opportunities for studying the functional activation of the brain, and has accelerated progress in many fields including neuroscience, psychology, and psychiatry. In studies involving NHPs, optical imaging techniques have been utilized to visualize functional modules in the cerebral cortex, and enabled the visualization of functional organization in visual, auditory, and somatosensory cortical areas [24,25]. Such visualization is made through monitoring variations in blood oxygenation driven by functionally specific neural activity and detecting the optical properties of tissue via either absorption or scattering. However, due to the overwhelming light scattering in brain tissue, high-resolution optical microscopy modalities can only monitor the surface of the exposed cortex; while diffuse optical modalities, although able to access subcortical brain region, have poor spatial resolution and limited depth information.

Ultrafast Doppler-based functional ultrasound imaging (fUS) has recently demonstrated some exciting capabilities of imaging cerebral blood volume (CBV) in NHPs [26]. However, it can only detect relatively large blood vessels with a flow speed above a certain detectable level, while its sensitivity to capillary flow is limited. In addition, blood oxygenation (sO_2), a vital measure of brain function, cannot be assessed by fUS.

The recently developed photoacoustic (PA) imaging (PAI) modality provides a unique solution to the above-mentioned barriers in NHP brain imaging. In contrast to conventional diffuse optical imaging methods, PAI has the unique capability to represent highly-sensitive optical information in deep brain tissues with excellent ultrasonic spatial resolution (better than 300 μm) at depths over 3 cm [27,28]. In previous research, the capability of PAI in mapping the structural and functional information in small-animal brains and monkey brains has been extensively studied [29–37]. PAI can quantitatively measure changes both in blood volume and blood oxygen saturation. The combination of these two measurements can directly assess the metabolic activities in brain tissues associated with brain functions. A PAI system has the potential to be mounted on the head of a monkey as a wearable device, without constraining any motion, to map brain function through a cranial window, and provide depth-resolved functional information in deep brain regions such as subcortical areas in real time with high spatial resolution.

The current study represents our initial results in applying PAI for real-time deep NHP brain imaging. For the first time, real-time photoacoustic computed tomography (PACT) was applied to image the subcortical region of a squirrel monkey through a cranial window when a forelimb digit was electrically stimulated. The hemodynamic responses of both cortical and subcortical brain regions underlying different cortices were monitored. Recent publication has demonstrated PACT through an intact human skull [38], where the imaging depth, however, was limited to the cortical regions. Therefore, NHP with a cranial window is still a necessary model for brain research and potential clinical translation. In addition, a photoacoustic microscopy (PAM) system was also used to detect the hemodynamic response on the cortical surface. Together, PAM and PACT provide a multi-scale mapping of the hemodynamic responses in the squirrel monkey brain during peripheral electrical stimulation.

2. Material and methods

2.1. Squirrel monkey preparation

Experiments were performed in two adult squirrel monkeys (*Saimiri scuireus*) aged approximately 12–15 years old. All procedures were done in accordance with protocols approved by the University of Kansas Institutional Care and Use Committee. All mapping and imaging were performed in a single procedure while the animal was anesthetized. Following completion of the data collection, monkeys were humanely euthanized and processed for post-mortem analysis.

2.1.1. Surgical procedures

Monkeys were initially anesthetized using ketamine (20–30 mg/kg i.m.) and atropine (0.04–0.07 mg/kg i.m.) and then prepared for surgery by shaving the head and forelimbs. Monkeys were intubated and gas anesthesia (70% nitrous oxide/30% oxygen plus 0.5–3% isoflurane to effect) was introduced and continued for the duration of the cranial opening. The saphenous vein was catheterized to allow for fluid delivery (10 ml/kg/hr of lactated Ringers with 3% dextrose). During the mapping and imaging procedures, ketamine was delivered (10–60 mg/kg/h i.v. in bolus doses of 2–6 mg, as needed) to maintain a steady anesthetic state. The head of the monkey was secured in a stereotaxic frame using earbars (Model 1430 Stereotaxic Frame, Kopf), and penicillin (G benzathine and G procaine 45,000 IU s.q.) was given. The incision area was infiltrated with bupivacaine (0.5–1.0 cc) and Mannitol (0.75–2 g/kg i.v.). Once body temperature and other vital signs were stable, surgery was initiated. The scalp over the right hemisphere was incised and reflected, the insertion of the temporalis muscle was cut, and a portion of the skull overlying the somatosensory and motor cortex was removed. The dura was incised and removed and a plastic cylinder (inner diameter: 2.5 cm) was affixed to the skull around the opening with dental acrylic.

2.1.2. Motor area mapping

To identify the motor areas of interest (primary motor cortex: M1; dorsal premotor cortex: PMd; ventral premotor cortex: PMv), we performed standard intracortical microstimulation (ICMS) mapping procedures [39–41]. A small, clear plastic ruler with 250 μm tick marks was placed on the surface of the cortex and the chamber was flooded with warm, sterile silicone oil to keep the surface from desiccating and to ease electrode insertion. A digital picture of the cortical surface vasculature was taken through the surgical microscope encompassing the entire cranial opening. The image was uploaded to a graphics suite (Canvas GFX Inc., Boston, MA). Distance within the program was calibrated to the cortical ruler, and a 250 μm grid was projected over the vascular image. Additional layers were added for recording responses to the microstimulation. A pulled glass micropipette (tapered to 15–20 μm o.d. tip and sharply beveled) filled with 3.5 M NaCl and fitted with a tungsten wire served as the microelectrode. It was inserted systematically into the cortex to a depth of 1750 μm ± 10 μm at grid intersections using the vascular pattern on the image as a fiducial reference. At each insertion site, a constant current stimulus isolator (Bak Electronics, Inc., Umatilla, FL) was used to inject a stimulus train (13 pulses of 200 μs duration pseudo-biphasic square waves at 330 Hz) at 1 Hz train intervals to visually observe evoked motor output. The stimulator was coupled to an audio amplifier so that stimulation pulse trains and movements could be visually correlated. Starting at 0 μA, current was ramped up (to a maximum of 30 μA) until a movement about a joint could be identified [40]. The movement type was then recorded on the digital image. The forelimb motor representations for primary and premotor cortex were mapped at roughly 500 μm resolution except at border locations or to differentiate M1 from PMd where the areas were mapped at 250–350 μm resolution.

2.1.3. Somatosensory area mapping

To derive somatosensory maps in S1, techniques for microelectrode recording of multiunit neuronal activity were used to define cutaneous and muscle/joint fields in areas 3a, 3b, and 1/2 [42–44]. The same digital image that was used to generate motor maps was used to co-register locations on the surface of the cortex for somatosensory maps. A 16-channel, single shank Michigan style probe (NeuroNexus Technologies part no. A1x16-100-703, Ann Arbor, MI) attached to a

unity-gain headstage and a digitizing amplifier (Tucker-Davis Technologies, Alachua, FL) was inserted into the somatosensory areas at ~ 1700 μA to span the entire cortical column at each location. Neural signals were piped to a computer workstation where they were filtered in real time and sent to an audio amplifier. Using visual analysis of the action potentials generated on each channel, one was selected based on rate of activity and the observed signal-to-noise ratio and was used to assess sensory responses. Minimal cutaneous receptive fields were defined by determining the skin field over which cortical neurons were driven by just visible indentation of the skin with a fine glass probe. Deep receptive fields were defined by high-threshold stimulation and joint manipulation. Two rostral-caudal rows of responses across D1 and D5 brain regions were taken to span from area 3a to area 2. This method allowed precise identification of borders between the somatosensory areas.

2.2. Peripheral electrical stimulation

To induce a peripheral response for imaging, pairs of 30 ga needle electrodes were subcutaneously inserted on the medial and lateral aspects of digit 2 parallel to the distal phalanges in each hand. These electrodes were connected to a constant current stimulus isolator (Bak Electronics, Inc., Umatilla, FL). For each trial, one finger was stimulated with 200 μs duration monophasic anodal pulses for 20 s at 1 Hz and an amplitude of either 3 or 8 mA. Current passed from the lateral electrode to the medial electrode. At these amplitudes, no reflexive movements correlated to the stimulation were observed.

2.3. Photoacoustic computed tomography (PACT) and photoacoustic microscopy (PAM) systems

Fig. 1a shows the schematic of the PACT system based on a linear array for the squirrel monkey brain imaging. An Nd:YAG laser (Surelight SLIII-10, Continuum, Santa Clara, CA) pumped optical parametric oscillator (OPO) (SLOPO Plus, Continuum, Santa Clara, CA) was used as the excitation source, with a pulse duration of 4–6 ns and a pulse repetition rate of 10 Hz. The laser beam at 797 nm was delivered through a bifurcated, multimode fiber bundle with fiber tips attached on both sides of a linear 128-element ultrasonic array (Verasonics L22–14v) with a central frequency of 15.6 MHz. This wavelength was chosen so that oxygenated and deoxygenated hemoglobin had the same absorption coefficients [45]. The maximum light intensity illuminated at the surface of the brain was ~ 20 mJ/cm^2, which is below the American National Standards Institute (ANSI) limit of 31 mJ/cm^2 at 797 nm. The resulting PA signals were detected by the ultrasonic array, which was placed vertically above the exposed right hemisphere for images in coronal view. The PA signals were acquired with a Vantage 128 ultrasound research system (Verasonics, Redmond, WA). The PACT imaging system had an axial resolution of 200 μm and a lateral resolution of 400 μm within 2 cm imaging depth [46].

For the PAM system (Fig. 1b), the excitation light of 532-nm wavelength was produced by a Q-switched diode pumped solid state (DPSS) laser (Elforlight Model SPOT-10–200–532, Bozeman, MT) with a pulse duration of 1.5 ns and a pulse repetition rate of 10 kHz. The pulse energy was 50 nJ and was focused by an objective lens (AC127-050-A, Thorlabs, Inc) onto the surface of the brain with 20 μm in diameter. A self-programmed Galvo mirror system was used to create a 5 mm × 5 mm scanning area (256 × 256 pixels). A calibrated needle hydrophone (HNC1500, ONDA Corp.) was placed near the scanning area to detect the generated PA signals. The temporal resolution of the PAM system was 10 s. Both 797 nm wavelength for PACT and 532 nm wavelength for PAM are isosbestic points, where deoxyhemoglobin and oxyhemoglobin have the same optical absorption.

2.4. Image reconstruction and signal processing

For each stimulation, 1 min spans (30 s before stimulation, 20 s of stimulation, and 10 s after stimulation) of monkey brain signals were acquired with the PACT system and reconstructed using a back-projection formula [47], resulting in a 600-frame time-lapsed PA recording. The 1 min PA recording was cross-correlated frame by frame and corrected for vertical motion induced by breathing of the monkey [48,49]. The temporal trace at each pixel was extracted from the PA recording. First, it was detrended by subtracting the linear fitting line of the pre-stimulation temporal trace to remove the systematic shift from the detected signal. Then, it was normalized by the root-mean-square of the signal strength of the original pre-stimulation temporal trace before subtraction. The resulting temporal trace is referred as the baseline-subtracted and normalized PA signals (ΔPA/PA). A spatial moving average of 3 × 3 pixels and a temporal forward-moving average of 25 frames (2.5 s) were also applied to filter out the noise from random fluctuations.

For the PAM system, the image was obtained by calculating the maximum intensity of the received ultrasound waves for each laser beam from the needle hydrophone. The intensities were calibrated by the directional response of the hydrophone based on the polar angles between the scanning points and the orientation of the transducer. The

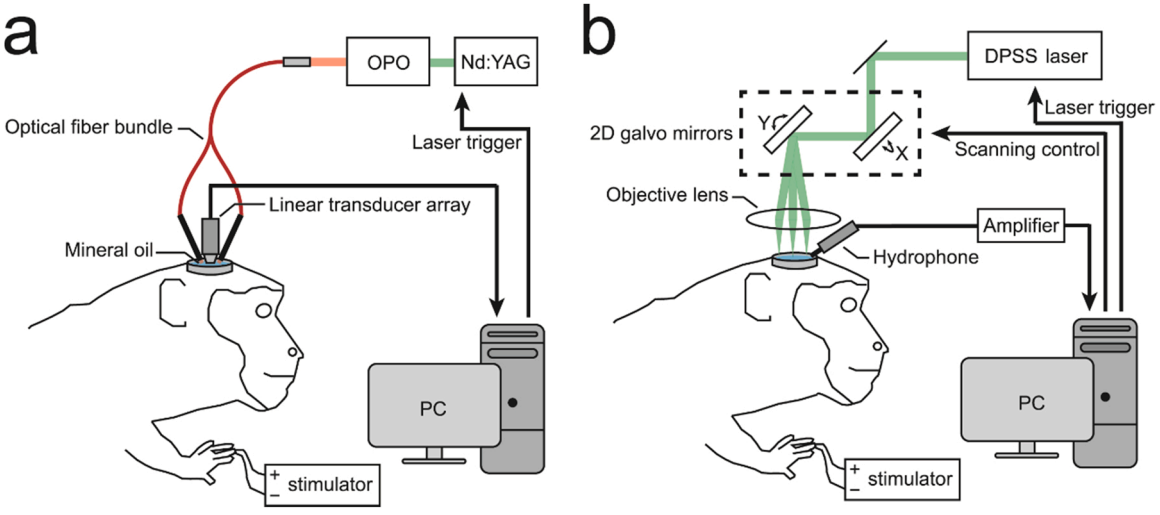

Fig. 1. Schematic diagrams of the photoacoustic imaging (PAI) system for squirrel monkeys with peripheral electrical stimulation. (a) Photoacoustic tomography (PACT) system. (b) Photoacoustic microscopy (PAM) system.

relative hemodynamic change of the PAM system was calculated by subtracting and dividing the post-stimulation image by the pre-stimulation image.

2.5. Magnetic resonance imaging (MRI) of the squirrel monkey brain

After the experiments, the squirrel monkey was euthanized, and the brain was harvested and fixed in 10% neutral buffered formalin (NBF). Then, MRI was used to co-register PA images with neuroanatomical locations. The T2-weighted MRI images of the monkey brain were acquired on a 7T Bruker Biospec MRI scanner (Bruker Inc., Billerica, MA) with turbo spin-echo (Rapid Acquisition with Refocused Echoes, RARE) based sequences (TR/TE = 2000/90 ms, 4 averages, RARE factor = 8, matrix = 256 × 256, field of view = 3.30 cm × 3.30 cm, number of slices = 50, slice thickness = 1 mm).

3. Results

3.1. Real-time PACT of the squirrel monkey brain in vivo

Before the PACT procedure, intracortical microstimulation (ICMS) was used to map the different cortical regions including the ventral premotor (PMv) and the dorsal premotor (PMd) cortices, the primary motor cortex (M1) and the primary somatosensory cortex (S1). During the experiments with the PACT system (Fig. 1a), the linear ultrasound transducer was placed at 3 different positions at the right hemisphere as indicated in Fig. 2a. PA images in coronal view at the level of the premotor cortices (slice 1), primary motor cortex (slice 2) and primary somatosensory cortex (slice 3) during peripheral electrical stimulation were then acquired (Fig. 2b–d). The subcortical region was identified on the T2-weighted MRI images based on the stereotaxic atlas of the squirrel monkey brain [50]. The identified regions were marked on the slices, including frontal gyrus (FG), precentral gyrus (PrG), postcentral gyrus (PoG), inferior parietal cortex (IPC), cauduate nucleus (Ca), internal capsule (IC), putamen (Put), and thalamus (Th). PA signals were produced predominantly from hemoglobin, indicating the blood vessel locations, which are primarily located subcortically beneath each coronal slice. The image obtained for each slice was reconstructed from the ultrasound transducer oriented vertically to the brain surface, providing only a single view of the imaging plane within the brain. Therefore, only vessels with normal orientation to the acoustic axis of the transducer could be clearly shown in the reconstructed images. Even though the structures of the other vessels might not be clear, the increase of their PA signals could still be reflected as the increase of the image background.

3.2. Temporal traces of electrically-evoked hemodynamic changes of different regions in cortical and subcortical brain structures

We next analyzed the temporal traces of PA signals in different regions. The temporal traces in each pixel of the temporal images were subtracted from the baseline (linear regression of the pre-stimulation phase) and normalized by the original signal strength of the baseline (the root mean square of the original pre-stimulation temporal trace) before subtraction, resulting in the baseline-subtracted and normalized PA signals (ΔPA/PA). To study the difference in responses from different cortical and subcortical regions, and to consider all of the vessels, including those with normal and deviated orientations due to the limited view of the reconstructed images, the temporal traces were averaged for different regions. The cortical regions included the gyrus regions (FG, PrG, PoG, IPC) and cerebral white matter, and subcortical regions (Ca, IC, Put, Th). After 8 mA electrical stimulation on the left index finger, the underlying tissue at the level of somatosensory cortex yielded strong hemodynamic changes in cortical areas (gyrus regions and cerebral white matter), which matched with the publications [51–53]. Though there were no limb movements of the monkey during stimulation, the electrical pulses may cause the contraction of limb muscles, and therefore activate weak hemodynamic changes in the cortical regions underlying the motor cortex and premotor cortices (20% and 12% weaker, respectively) (Fig. 3a, c). Due to the optical and acoustic attenuation through cortical tissues, the responses in subcortical areas underlying the somatosensory cortex, motor cortex and premotor cortices were 44–64% smaller than that in cortical areas (Fig. 3a, c, e). Stimulation level also contributed to different levels of response. All 3 cortices generated weaker (19%–37%) responses for 3 mA stimulation compared to 8 mA stimulation (Fig. 3b, d, and f).

3.3. Temporal traces of electrically-evoked hemodynamic change of single vessels in the cortical brain

In each slice, we identified two primary vessels in the white matter that had the strongest PA signal amplitude, shown in Fig. 4 (marked from 1 to 6 in Fig. 2b–d). Some vessels were observed to have stronger

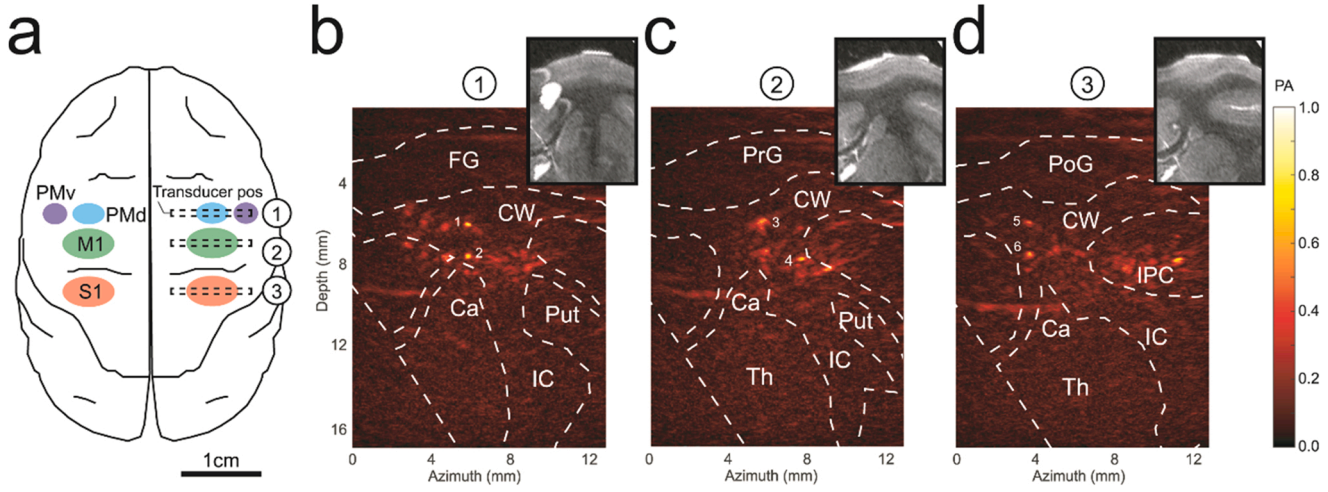

Fig. 2. (a) Cerebral cortex regions including premotor cortex (PMd, PMv), primary motor cortex (M1) and primary somatosensory cortex (S1). (b) PACT images of the right hemisphere at PMd and PMv, (c) M1 and S1, and corresponding MRI images at each region. The transducer positions for (b–d) are shown in (a). FG: frontal gyrus, PrG: precentral gyrus, PoG: postcentral gyrus, IPC: inferior parietal cortex, CW: cerebral white matter, Ca: caudate nucleus, IC: internal capsule, Put: putamen, Th: thalamus. The colormap represents the normalized PA amplitude. (For interpretation of the references to color in this figure legend, the reader is referred to the web version of this article.)

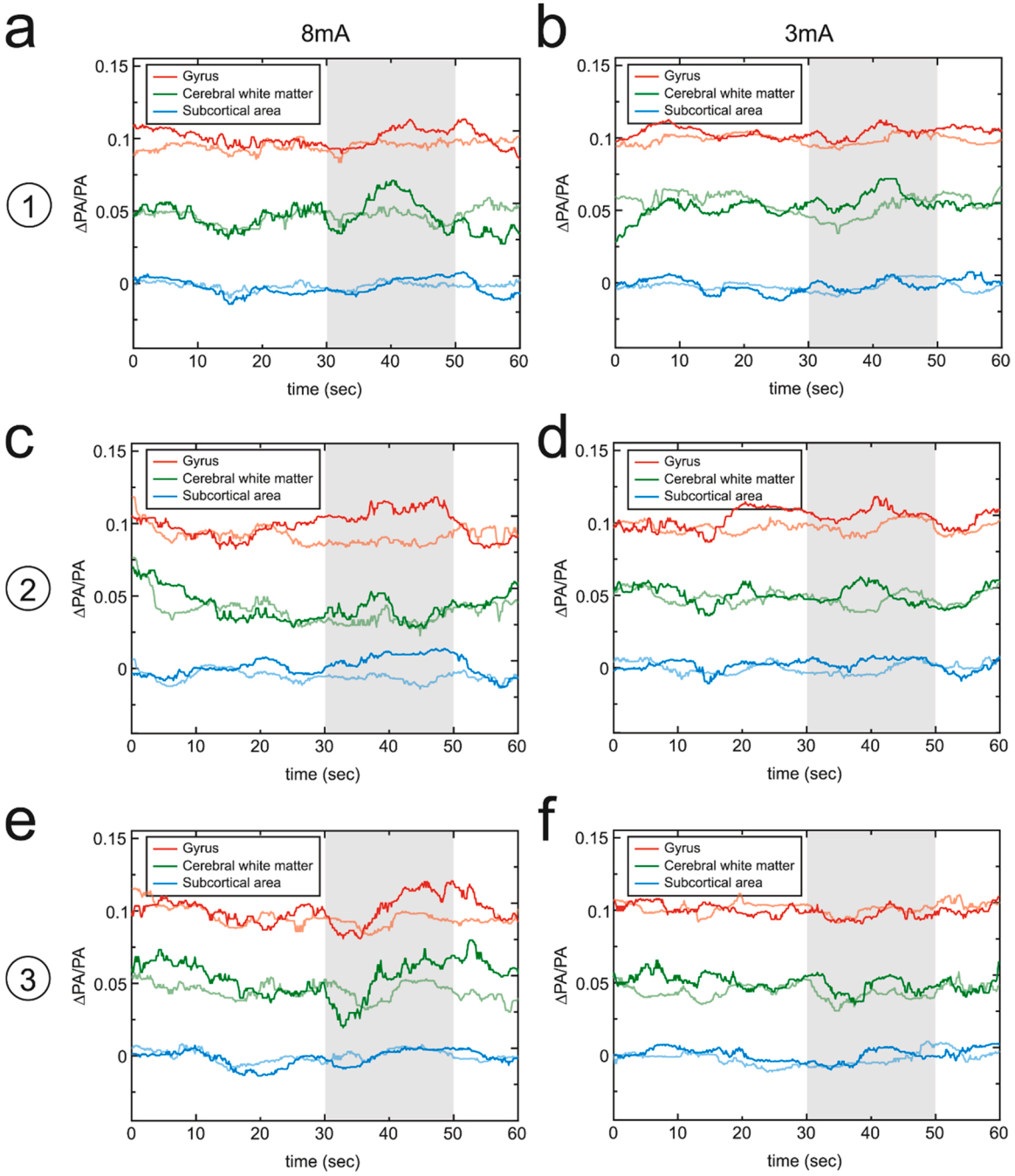

Fig. 3. PACT imaging of electrically-evoked hemodynamic change in vivo. The temporal traces of the baseline-subtracted and normalized PA signals (ΔPA/PA) for cortical, including gyrus (FG, PrG, PoG, IPC) and cerebral white matter (CW), and subcortical (Ca, IC, Put, Th) brain regions at PMd and PMv of the right hemisphere with electrical stimulation of (a) 8 mA and (b) 3 mA on the left hand index finger. (c, d) The temporal traces of different brain regions at M1 with electrical stimulation of 8 mA and 3 mA, respectively. (e, f) The temporal traces of different brain regions at S1 with electrical stimulation of 8 mA and 3 mA. The light red, green, and blue lines indicate the temporal traces with electrical stimulation on the right hand index finger (control). Shaded area represents the time period of the stimulation. (For interpretation of the references to color in this figure legend, the reader is referred to the web version of this article.)

responses than the regional analysis in Fig. 3, such as vessel 1 and vessel 4 under 8 mA electrical stimulation. Most vessels had similar levels of responses, but there was almost no response for vessel 3 under 8 mA electrical stimulation in comparison with the regional analysis of gyrus regions of slice 2. This indicated that single vessel analysis had potential to reveal the vessels contributing to the response in the white matter and higher hemodynamic responses might be obtained. However, not all the primary vessels (vessels with strong PA signals) contributed to the responses in the white matter.

3.4. Functional imaging by hemodynamic change during electrical stimulation

Functional images were obtained by calculating the relative variations of the averaged signal amplitude in each pixel of the temporal PA images during stimulation (30–50 s) compared to the averaged signal amplitude before stimulation (0–30 s). Areas with relative variation greater than 0.5% (average relative variation in control groups) were marked from yellow to red color on the grayscale PA images, showing areas with hemodynamic responses during electrical stimulation

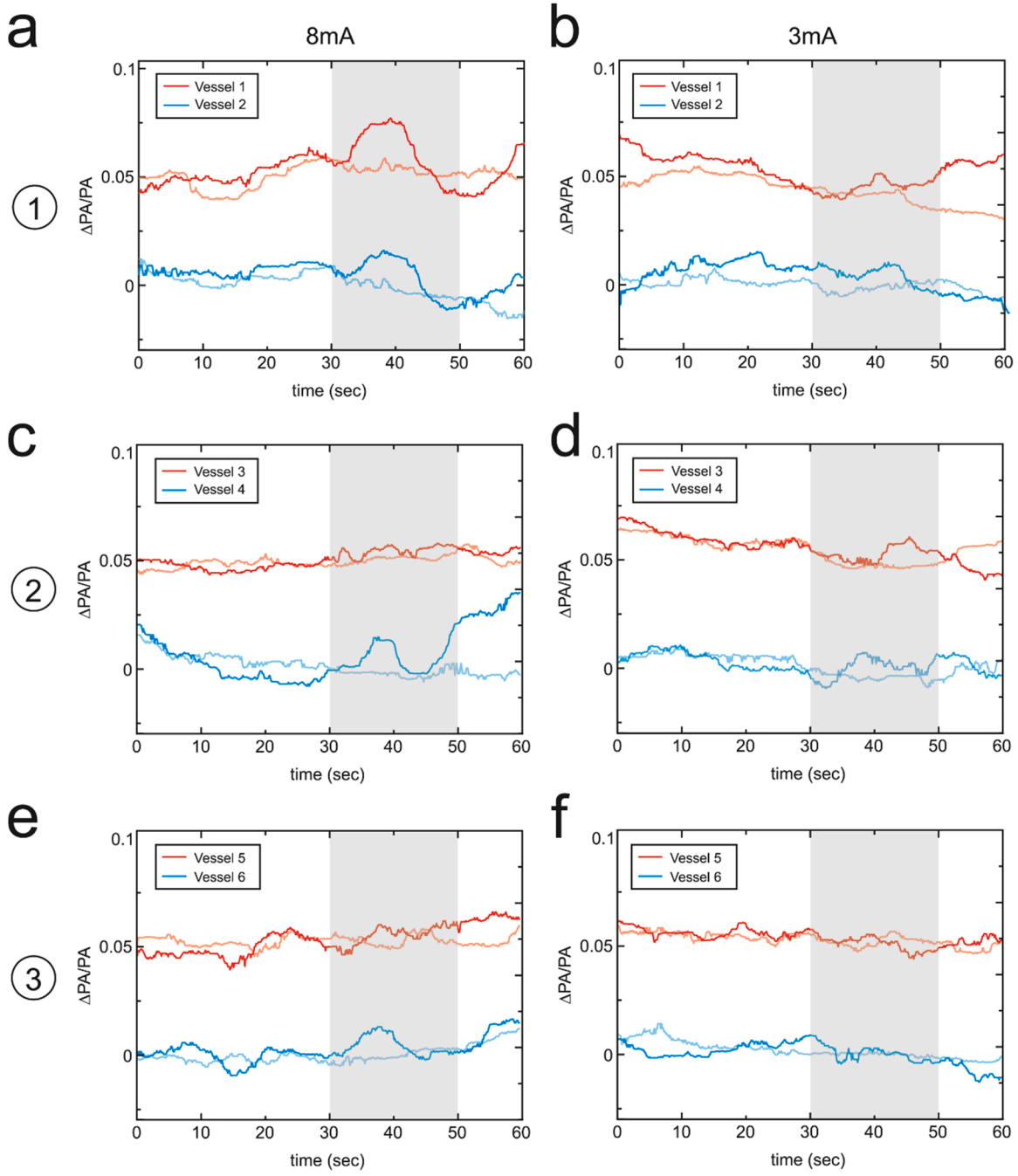

Fig. 4. Temporal traces electrically-evoked hemodynamic changes in single blood vessels in vivo. The temporal traces of the baseline-subtracted and normalized PA signals (ΔPA/PA) for the two vessels with the highest signal strength at the level of PMd and PMv of the right hemisphere with electrical stimulation of (a) 8 mA and (b) 3 mA on the left hand index finger. (c, d) The temporal traces of the two strongest vessels at the level of M1 with electrical stimulation of 8 mA and 3 mA, respectively. (e, f) The temporal traces of the two strongest vessels at the level of S1 with electrical stimulation of 8 mA and 3 mA, respectively. The vessel positions are shown in Fig. 2. The light red, green and blue lines indicate the temporal traces with electrical stimulation on the right hand index finger (control). Shaded area represents the time period of the stimulation. (For interpretation of the references to color in this figure legend, the reader is referred to the web version of this article.)

(Fig. 5). Most of the areas with strong hemodynamic change were located in the white matter, less were in the gyrus regions, and functional changes in the subcortical regions were the weakest. These functional images showed the pixels of vessels responding to the peripheral electrical stimulation.

3.5. Photoacoustic microscopy (PAM) imaging in the primary somatosensory cortex (S1)

The highly sensitive photoacoustic microscopy (PAM, Fig. 1b) was utilized to examine S1 shown in Fig. 6a in order to demonstrate the multiscale potential of photoacoustic imaging technology. The vasculature in the generated PAM image (Fig. 6b) matched with the photograph shown in Fig. 6a except for the bottom left corner where the laser light was out of focus due to the curved surface of the brain. The relative

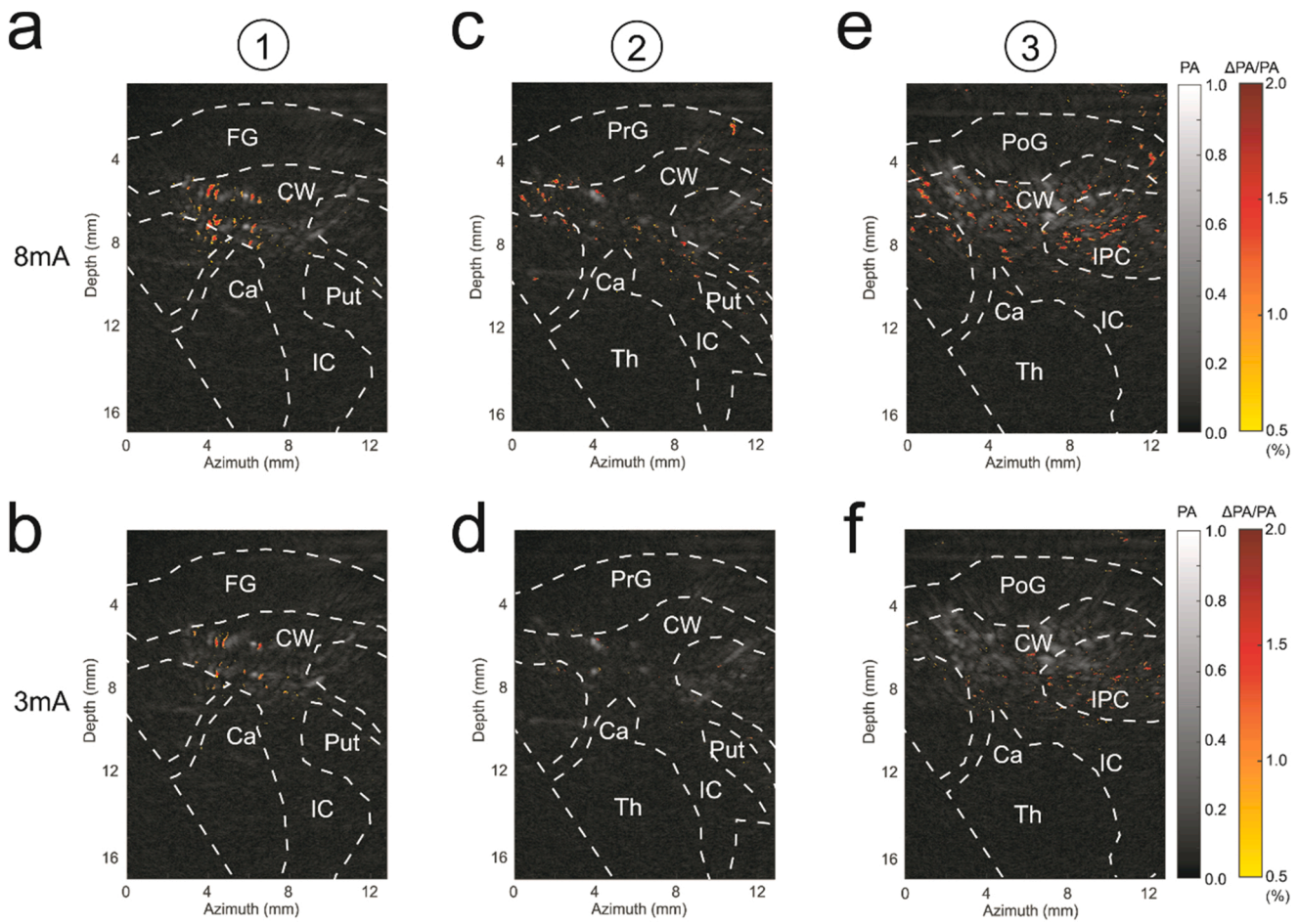

Fig. 5. Functional imaging by electrically-evoked hemodynamic change before and during the stimulation. The regions at the level of PMd and PMv of the right hemisphere under electrical stimulation (grayscale) of (a) 8 mA and (b) 3 mA with the relative variation of the average signals during the stimulation to the average signals before the stimulation. (c, d) The regions with the relative variation at the level of M1 with electrical stimulation of 8 mA and 3 mA, respectively. (e, f) The regions with the normalized variation at the level of S1 with electrical stimulation of 8 mA and 3 mA, respectively. The colormap represents the normalized PA amplitude and relative amplitude variation, respectively. (For interpretation of the references to color in this figure legend, the reader is referred to the web version of this article.)

PA signal of hemodynamic change was then calculated by subtracting the PA signal before the electrical stimulation and then normalized. The relative change with 8 mA electrical stimulation was high at the origin of the primary vessels and became lower along the microvessels (Fig. 6c). Similar to the PACT results, the relative change was much smaller (74% weaker) with 3 mA electrical stimulation than that with 8 mA electrical stimulation. The results in the above demonstrated that the electrically-evoked hemodynamic change during the stimulation could be observed with both PACT and PAM imaging setup. PACT was able to provide information in deep (~ 16 mm) brain regions with high temporal resolution (10 Hz). PAM, on the other hand, featured high resolution vasculature and was more sensitive to the hemodynamic response.

4. Discussion and conclusion

In summary, we have built a linear-array PACT system for imaging subcortical regions and a high-resolution PAM system for imaging cortical areas of the brain of the squirrel monkey. We investigated the hemodynamic responses of multiple cortical areas to peripheral electrical stimulation by monitoring the changes in blood volume in vessels. Strong cortical responses were observed in both cortical and subcortical brain regions within coronal slices at the level of the premotor cortices under 8 mA electrical stimulation. Temporal profiles of electrically-evoked hemodynamic responses were characterized in individual blood vessels several millimeters below the cortical surface. Responses within coronal slices at the level of primary motor and somatosensory cortex were also observed, but were weaker. Responses were also weaker with lower stimulation currents (3 mA). Although the PAM system has shallow tissue penetration and is not applicable for transcranial imaging in non-human primates, the PAM system demonstrated better sensitivity and higher resolution to observe the hemodynamic response to stimulation in the cortical areas. The initial results from the monkey brain in vivo validated the potential of PAI technique for multiscale and multi-resolution mapping of brain functions.

The temporal resolution (~ 10 s) of the current PAM system is relatively low. This limitation can be addressed by employing a higher repetition-rate laser for PA excitation. Though signal detection through a cranial window is a standard approach in brain research with non-human primates, if detection with an intact skull is desired for future application, the skull aberrations in the PACT system could be potentially reduced using excitation laser with longer wavelength (e.g., 1064 nm) and ultrasound transducer with lower central frequency (e.g., 1 MHz) to compromise both optical attenuation and acoustic aberration [38,54]. The imaging depth and resolution can also be improved by providing multiple views of the brain using the linear array [55]. Besides using the blood volume of vessels for monitoring hemodynamic changes, PAI systems utilizing multiple laser wavelengths have the potential for detecting the change in blood oxygenation (sO_2) as another measure of the cortical response to stimulation [56,57].

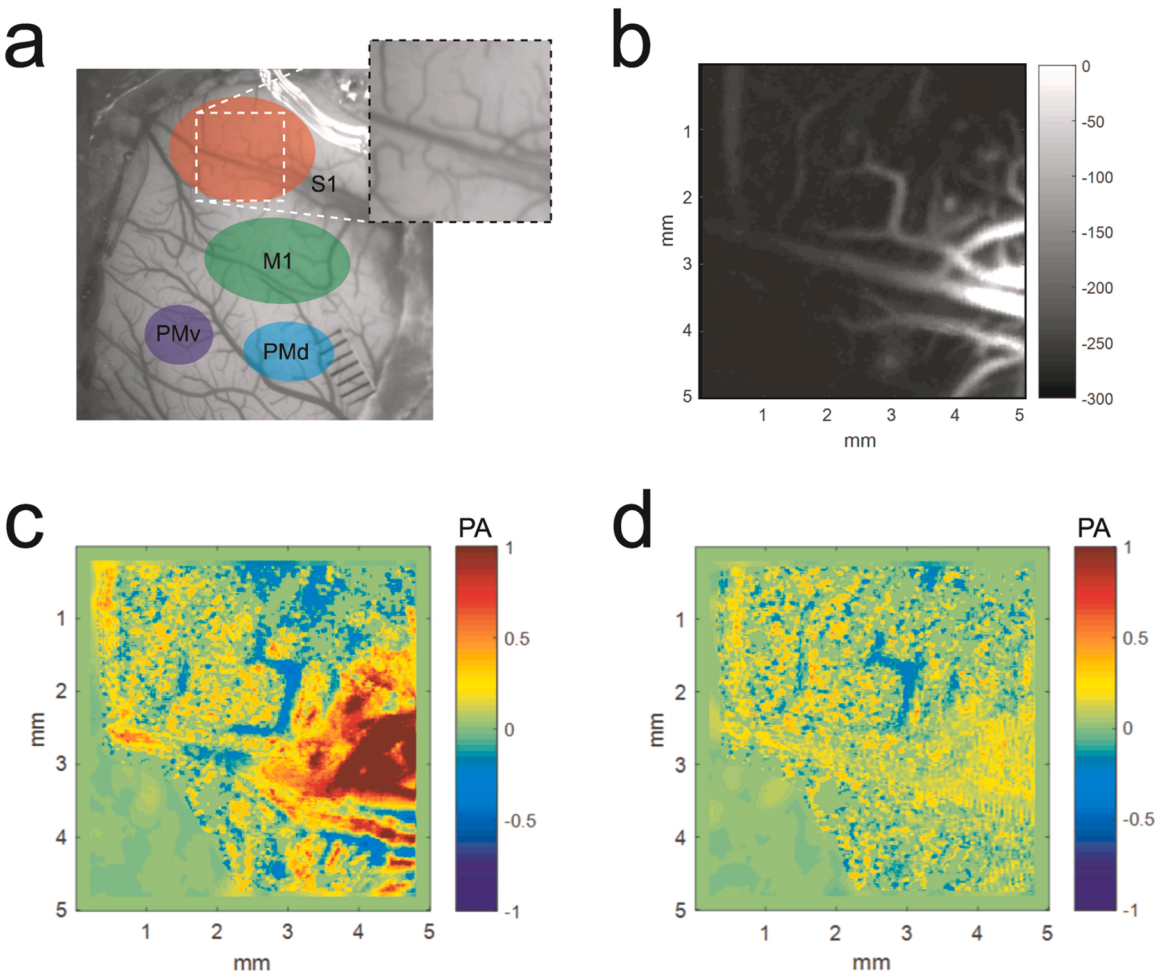

Fig. 6. PAM imaging of electrically-evoked hemodynamic change. (a) Cerebral cortex regions shown on the photograph of the squirrel monkey brain. (b) The PAM image at S1. The relative change of hemodynamic signals at S1 after electrical stimulation of (c) 8 mA and (d) 3 mA. The colormap represents the normalized relative PA signal change.

Declaration of Competing Interest

The authors declare that they have no known competing financial interests or personal relationships that could have appeared to influence the work reported in this paper.

Acknowledgments

This research was supported in part by National Institute of Health, United States (R01NS118918 and R01NS030853).

References

[1] K.A. Phillips, K.L. Bales, J.P. Capitanio, A. Conley, P.W. Czoty, B.A. t Hart, W. D. Hopkins, S.-L. Hu, L.A. Miller, M.A. Nader, P.W. Nathanielsz, J. Rogers, C. A. Shively, M.L. Voytko, Why primate models matter, Am. J. Primatol. 76 (9) (2014) 801–827.

[2] G.A. Orban, D. Van Essen, W. Vanduffel, Comparative mapping of higher visual areas in monkeys and humans, Trends Cogn. Sci. 8 (7) (2004) 315–324.

[3] S. Sani, D. Traul, A. Klink, N. Niaraki, A. Gonzalo-Ruiz, C.K. Wu, C. Geula, Distribution, progress and chemical composition of cortical amyloid-beta deposits in aged rhesus monkeys: similarities to the human, Acta Neuropathol. 105 (2) (2003) 145–156.

[4] D. Koshiyama, M. Fukunaga, N. Okada, F. Yamashita, H. Yamamori, Y. Yasuda, M. Fujimoto, K. Ohi, H. Fujino, Y. Watanabe, K. Kasai, R. Hashimoto, Role of subcortical structures on cognitive and social function in schizophrenia, Sci. Rep. 8 (1) (2018) 1183.

[5] P.M. Matthews, G.D. Honey, E.T. Bullmore, Applications of fMRI in translational medicine and clinical practice, Nat. Rev. Neurosci. 7 (9) (2006) 732–744.

[6] N.K. Logothetis, What we can do and what we cannot do with fMRI, Nature 453 (7197) (2008) 869–878.

[7] J. Hua, R.D. Stevens, A.J. Huang, J.J. Pekar, P.C.M. van Zijl, Physiological origin for the BOLD poststimulus undershoot in human brain: vascular compliance versus oxygen metabolism, J. Cereb. Blood Flow Metab. 31 (7) (2011) 1599–1611.

[8] J.M. Lawrence, J. Kornelsen, P.W. Stroman, Noninvasive observation of cervical spinal cord activity in children by functional MRI during cold thermal stimulation, Magn. Reson. Imaging 29 (6) (2011) 813–818.

[9] A. Van der Linden, N. Van Camp, P. Ramos-Cabrer, M. Hoehn, Current status of functional MRI on small animals: application to physiology, pathophysiology, and cognition, NMR Biomed. 20 (5) (2007) 522–545.

[10] K.M. Vogt, J.W. Ibinson, P. Schmalbrock, R.H. Small, The impact of physiologic noise correction applied to functional MRI of pain at 1.5 and 3.0 T, Magn. Reson. Imaging 29 (6) (2011) 819–826.

[11] J. Pfeuffer, A. Shmuel, G.A. Keliris, T. Steudel, H. Merkle, N.K. Logothetis, Functional MR imaging in the awake monkey: effects of motion on dynamic off-resonance and processing strategies, Magn. Reson. Imaging 25 (6) (2007) 869–882.

[12] G. Chen, F. Wang, B.C. Dillenburger, R.M. Friedman, L.M. Chen, J.C. Gore, M. J. Avison, A.W. Roe, Functional magnetic resonance imaging of awake monkeys: some approaches for improving imaging quality, Magn. Reson. Imaging 30 (1) (2012) 36–47.

[13] P.D. Gamlin, M.K. Ward, M.S. Bolding, J.K. Grossmann, D.B. Twieg, Developing functional magnetic resonance imaging techniques for alert macaque monkeys, Methods 38 (3) (2006) 210–220.

[14] J.B.M. Goense, K. Whittingstall, N.K. Logothetis, Functional magnetic resonance imaging of awake behaving macaques, Methods 50 (3) (2010) 178–188.

[15] M.A. Pinsk, T. Moore, M.C. Richter, C.G. Gross, S. Kastner, Methods for functional magnetic resonance imaging in normal and lesioned behaving monkeys, J. Neurosci. Methods 143 (2) (2005) 179–195.

[16] T. Durduran, M.G. Burnett, G.Q. Yu, C. Zhou, D. Furuya, A.G. Yodh, J.A. Detre, J. H. Greenberg, Spatiotemporal quantification of cerebral blood flow during functional activation in rat somatosensory cortex using laser-speckle flowmetry, J. Cereb. Blood Flow Metab. 24 (5) (2004) 518–525.

[17] S. Yuan, A. Devor, D.A. Boas, A.K. Dunn, Determination of optimal exposure time for imaging of blood flow changes with laser speckle contrast imaging, Appl. Opt. 44 (10) (2005) 1823–1830.
[18] S.A. Sheth, M. Nemoto, M. Guiou, M. Walker, N. Pouratian, A.W. Toga, Linear and nonlinear relationships between neuronal activity, oxygen metabolism, and hemodynamic responses, Neuron 42 (2) (2004) 347–355.
[19] A.P. Gibson, J.C. Hebden, S.R. Arridge, Recent advances in diffuse optical imaging, Phys. Med. Biol. 50 (4) (2005) R1–R43.
[20] J.P. Culver, A.M. Siegel, J.J. Stott, D.A. Boas, Volumetric diffuse optical tomography of brain activity, Opt. Lett. 28 (21) (2003) 2061–2063.
[21] G. Strangman, D.A. Boas, J.P. Sutton, Non-invasive neuroimaging using near-infrared light, Biol. Psychiatry 52 (7) (2002) 679–693.
[22] P.B. Jones, H.K. Shin, D.A. Boas, B.T. Hyman, M.A. Moskowitz, C. Ayata, A. K. Dunn, Simultaneous multispectral reflectance imaging and laser speckle flowmetry of cerebral blood flow and oxygen metabolism in focal cerebral ischemia, J. Biomed. Opt. 13 (4) (2008).
[23] B.W. Zeff, B.R. White, H. Dehghani, B.L. Schlaggar, J.P. Culver, Retinotopic mapping of adult human visual cortex with high-density diffuse optical tomography, Proc. Natl. Acad. Sci. USA 104 (29) (2007) 12169–12174.
[24] A. Grinvald, R.D. Frostig, R.M. Siegel, E. Bartfeld, High-resolution optical imaging of functional brain architecture in the awake monkey, Proc. Natl. Acad. Sci. USA 88 (24) (1991) 11559–11563.
[25] N. Vnek, B.M. Ramsden, C.P. Hung, P.S. Goldman-Rakic, A.W. Roe, Optical imaging of functional domains in the cortex of the awake and behaving monkey, Proc. Natl. Acad. Sci. USA 96 (7) (1999) 4057–4060.
[26] A. Dizeux, M. Gesnik, H. Ahnine, K. Blaize, F. Arcizet, S. Picaud, J.A. Sahel, T. Deffieux, P. Pouget, M. Tanter, Functional ultrasound imaging of the brain reveals propagation of task-related brain activity in behaving primates, Nat. Commun. 10 (1) (2019) 1400.
[27] C. Kim, T.N. Erpelding, L. Jankovic, M.D. Pashley, L.V. Wang, Deeply penetrating in vivo photoacoustic imaging using a clinical ultrasound array system, Biomed. Opt. Express 1 (1) (2010) 278–284.
[28] G. Ku, L.H.V. Wang, Deeply penetrating photoacoustic tomography in biological tissues enhanced with an optical contrast agent, Opt. Lett. 30 (5) (2005) 507–509.
[29] E.W. Stein, K. Maslov, L.V. Wang, Noninvasive Mapping of the Electrically Stimulated Mouse Brain Using Photoacoustic Microscopy, SPIE, San Jose, 2008, 68561J-68561J.
[30] X.D. Wang, Y.J. Pang, G. Ku, X.Y. Xie, G. Stoica, L.H.V. Wang, Noninvasive laser-induced photoacoustic tomography for structural and functional in vivo imaging of the brain, Nat. Biotechnol. 21 (7) (2003) 803–806.
[31] X.M. Yang, L.V. Wang, Monkey brain cortex imaging by photoacoustic tomography, J. Biomed. Opt. 13 (4) (2008), 044009.
[32] J. Jo, H. Zhang, P.D. Cheney, X. Yang, Photoacoustic detection of functional responses in the motor cortex of awake behaving monkey during forelimb movement, J. Biomed. Opt. 17 (11) (2012), 110503-110503.
[33] J. Staley, P. Grogan, A.K. Samadi, H.Z. Cui, M.S. Cohen, X.M. Yang, Growth of melanoma brain tumors monitored by photoacoustic microscopy, J. Biomed. Opt. 15 (4) (2010). Article No. 040510.
[34] J. Jo, X. Yang, Detection of cocaine induced rat brain activation by photoacoustic tomography, J. Neurosci. Methods 195 (2) (2011) 232–235.
[35] X.M. Yang, A. Maurudis, J. Gamelin, A. Aguirre, Q. Zhu, L.V. Wang, Photoacoustic tomography of small animal brain with a curved array transducer, J. Biomed. Opt. 14 (5) (2009), 054007.
[36] X. Yang, A. Maurudis, J. Gamelin, A. Aguirre, Q. Zhu, L.V. Wang, Photoacoustic tomography of small animal brain with a curved array transducer, J. Biomed. Opt. 14 (5) (2009), 054007.
[37] Y. Liu, H. Liu, H. Yan, Y. Liu, J. Zhang, W. Shan, P. Lai, H. Li, L. Ren, Z. Li, L. Nie, Aggregation-induced absorption enhancement for deep near-infrared II photoacoustic imaging of brain gliomas in vivo, Adv. Sci. 6 (8) (2019), 1801615.
[38] S. Na, J.J. Russin, L. Lin, X. Yuan, P. Hu, K.B. Jann, L. Yan, K. Maslov, J. Shi, D. J. Wang, C.Y. Liu, L.V. Wang, Massively parallel functional photoacoustic computed tomography of the human brain, Nat. Biomed. Eng. (2021).
[39] S.B. Frost, S. Barbay, K.M. Friel, E.J. Plautz, R.J. Nudo, Reorganization of remote cortical regions after ischemic brain injury: a potential substrate for stroke recovery, J. Neurophysiol. 89 (6) (2003) 3205–3214.
[40] R.J. Nudo, W.M. Jenkins, M.M. Merzenich, T. Prejean, R. Grenda, Neurophysiological correlates of hand preference in primary motor cortex of adult squirrel monkeys, J. Neurosci. 12 (8) (1992) 2918–2947.
[41] R.J. Nudo, G.W. Milliken, Reorganization of movement representations in primary motor cortex following focal ischemic infarcts in adult squirrel monkeys, J. Neurophysiol. 75 (5) (1996) 2144–2149.
[42] N. Dancause, S. Barbay, S.B. Frost, E.J. Plautz, D. Chen, E.V. Zoubina, A.M. Stowe, R.J. Nudo, Extensive cortical rewiring after brain injury, J. Neurosci. 25 (44) (2005) 10167–10179.
[43] R.J. Nudo, Remodeling of cortical motor representations after stroke: implications for recovery from brain damage, Mol. Psychiatry 2 (3) (1997) 188–191.
[44] S. Barbay, E.K. Peden, G. Falchook, R.J. Nudo, Sensitivity of neurons in somatosensory cortex (S1) to cutaneous stimulation of the hindlimb immediately following a sciatic nerve crush, Somatosens. Mot. Res. 16 (2) (1999) 103–114.
[45] J. Tang, L. Xi, J. Zhou, H. Huang, T. Zhang, P.R. Carney, H. Jiang, Noninvasive high-speed photoacoustic tomography of cerebral hemodynamics in awake-moving rats, J. Cereb. Blood Flow Metab. Off. J. Int. Soc. Cereb. Blood Flow Metab. 35 (8) (2015) 1224–1232.
[46] K. Kratkiewicz, R. Manwar, Y. Zhou, M. Mozaffarzadeh, K. Avanaki, Technical considerations in the Verasonics research ultrasound platform for developing a photoacoustic imaging system, Biomed. Opt. Express 12 (2) (2021) 1050–1084.
[47] M. Xu, L.V. Wang, Universal back-projection algorithm for photoacoustic computed tomography, Phys. Rev. E 71 (1) (2005), 016706.
[48] J. Aguirre, A. Berezhnoi, H. He, M. Schwarz, B. Hindelang, M. Omar, V. Ntziachristos, Motion quantification and automated correction in clinical RSOM, IEEE Trans. Med. Imaging 38 (6) (2019) 1340–1346.
[49] M. Schwarz, N. Garzorz-Stark, K. Eyerich, J. Aguirre, V. Ntziachristos, Motion correction in optoacoustic mesoscopy, Sci. Rep. 7 (1) (2017) 10386.
[50] J.A. Gergen, P.D. MacLean, National Institutes of Health. A Stereotaxic Atlas of the Squirrel Monkey's Brain (Saimiri sciureus), U.S. Department of Health, Education, and Welfare, Public Health Service, National Institutes of Health, Bethesda, Md., 1962.
[51] R. Anna Wang, E.W. Jeremy, M.F. Robert, Study of single and multidigit activation in monkey somatosensory cortex using voltage-sensitive dye imaging, Neurophotonics 4 (3) (2017) 1–9.
[52] R. Wu, L. Su, P.-F. Yang, L. Min Chen, Altered spatiotemporal dynamics of cortical activation to tactile stimuli in somatosensory area 3b and area 1 of monkeys after spinal cord injury, eNeuro 3 (5) (2016). ENEURO.0095-16.2016.
[53] L.M. Chen, G.H. Turner, R.M. Friedman, N. Zhang, J.C. Gore, A.W. Roe, M. J. Avison, High-resolution maps of real and illusory tactile activation in primary somatosensory cortex in individual monkeys with functional magnetic resonance imaging and optical imaging, J. Neurosci. 27 (34) (2007) 9181.
[54] L. Nie, X. Cai, K. Maslov, A. Garcia-Uribe, M.A. Anastasio, L.V. Wang, Photoacoustic tomography through a whole adult human skull with a photon recycler, J. Biomed. Opt. 17 (11) (2012), 110506.
[55] P. Zhang, L. Li, L. Lin, P. Hu, J. Shi, Y. He, L. Zhu, Y. Zhou, L.V. Wang, High-resolution deep functional imaging of the whole mouse brain by photoacoustic computed tomography in vivo, J. Biophotonics 11 (1) (2018), e201700024.
[56] M. Li, Y. Tang, J. Yao, Photoacoustic tomography of blood oxygenation: a mini review, Photoacoustics 10 (2018) 65–73.
[57] W.S. Erich, I.M. Konstantin, V.W. Lihong, Noninvasive, in vivo imaging of blood-oxygenation dynamics within the mouse brain using photoacoustic microscopy, J. Biomed. Opt. 14 (2) (2009) 1–3.

Kai-Wei Chang is a Ph.D. candidate at Department of Biomedical Engineering in the University of Michigan. He received his M.S. degree in biomedical electronics and bioinformatics and B.S. degree in electrical engineering from National Taiwan University. His current research focuses on photoacoustic imaging and multi-modality brain imaging.

Yunhao Zhu received the Ph.D. degree and B.S. degree in electronic science and engineering from Nanjing University, China. From 2016–2020, he was a visiting scholar at Optical Imaging Lab, University of Michigan—Ann Arbor, USA. His research included the studies of Crohn's disease detection with photoacoustic imaging, LED-based photoacoustic imaging and potential clinical applications, full-wave inversion 3D speed of sound image reconstruction, and brain imaging using photoacoustic computed tomography, bone assessment through photoacoustic and ultrasound techniques. During his Ph.D. period, he has published several papers on peer-review journals as the first author, including Gastroenterology, Scientific Reports, Biomedical optics express, Sensors, etc. and a book chapter.

Heather M. Hudson received the Ph.D. degree at University of Kansas Medical Center and is now a senior scientist of the Landon Center on Aging at University of Kansas Medical Center. Her research interest is cortical plasticity.

Scott Barbay is a senior scientist at Landon Center on Aging, University of Kansas Medical Center, Kansas City. His research interests include translational models of stroke recovery that emphasize neurophysiological and neuroanatomical reorganization within the cerebral cortex associated with recovery of motor function after stroke.

David J. Guggenmos is a research assistant professor at the University of Kansas Medical Center. He received the B.S. degree in psychology from Iowa State University and the Ph.D. degree at the University of Kansas Medical Center. His research interests include motor cortical plasticity and the effects of electrical stimulation on neural tissue.

Dr. Randolph J. Nudo is a University Distinguished Professor & Vice Chair of Research, Department of Rehabilitation Medicine and the Director of the Landon Center on Aging. As Director of the Landon Center on Aging, Dr. Nudo is responsible for fiscal management of the Center on Aging, coordination of interdisciplinary education, research and service activities, and the development of new programs devoted to the health and well-being of older Kansans. He is also Director of the Institute for Neurological Discoveries, dedicated to developing solutions to the growing number of neurological disorders occurring in the United States. He serves as the Marion Merrell Dow Distinguished Professor in Aging. Dr. Nudo's Cortical Plasticity Laboratory focuses on understanding the brain's self-repair capacity after injury, and developing novel therapeutic approaches based on neuroscientific principles. Dr. Nudo is Principal Investigator on an NIH funded project to study neural mechanisms of functional recovery after stroke. This grant has had continuous funding since 1993. His research focuses on translating basic science research into more effective clinical interventions for neurological disorders that accompany aging. He is recognized internationally for his work on the effects of rehabilitative training on functional plasticity after stroke, and is a frequent speaker at national and international symposia on stroke, neurology, neuroengineering and physical therapy and rehabilitation.

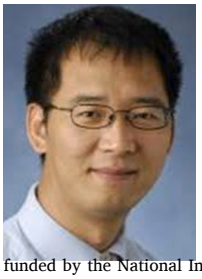

Dr. Xinmai Yang is a Associate Professor at the Department of Mechanical Engineering, University of Kansas. He was previously a postdoctoral research associate at Washington University in St. Louis from 2006 to 2008. He has also worked at the National Center for Physical Acoustics at the University of Mississippi as a postdoctoral fellow. Dr. Yang conducts research in photoacoustic imaging and biomedical applications of ultrasound. He has authored or co-authored over 40 peer-reviewed journal articles and conference proceeding publications. Dr. Yang's research focuses on early cancer detection, as well as molecular imaging and brain functional imaging with both optical and/or ultrasound methods. His research has been funded by the National Institutes of Health. Dr. Yang is a member of Society of Photographic Instrumentation Engineers, and is an associate member of the Acoustical Society of America.

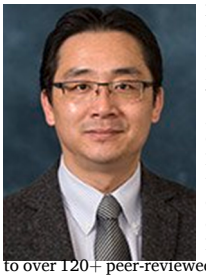

Dr. Xueding Wang is a Professor at the Department of Biomedical Engineering, University of Michigan, holding an adjunct Professor position at the Department of Radiology. Before working as an independent principal investigator, Dr. Wang received his Ph.D. from the Dwight Look College of Engineering at Texas A&M University, and then finished postdoctoral training at the University of Michigan School of Medicine. Dr. Wang has extensive experience in imaging system development and adaptation of novel diagnostic technology to laboratory research and clinical managements, especially those involving light and ultrasound. Sponsored by NIH, NSF, DoD and other funding agencies, his research has led to over 120+ peer-reviewed publications. At the University of Michigan Medical School, a major part of his research is focused on clinical applications of photoacoustic imaging, including those involving arthritis, prostate cancer, liver conditions, breast cancer, Crohn's disease, and eye diseases. Dr. Wang is the recipient of the Sontag Foundation Fellow of the Arthritis National Research Foundation in 2005, and the Distinguished Investigator Award of the Academy of Radiology Research in 2013. He is also sitting on the editorial boards of scientific journals including Photoacoustics, Journal of Biomedical Optics, Medical Physics, and Ultrasonic Imaging, and being the steering committee member of the Journal of Lightwave Technology.